Advanced Composite Materials
Publication details, including instructions for authors and subscription information:
http://www.tandfonline.com/loi/tacm20

Smart Honeycomb Sandwich Panels With Damage Detection and Shape Recovery Functions

Yoji Okabe [a], Shu Minakuchi [b], Nobuo Shiraishi [c], Ken Murakami [d] & Nobuo Takeda [e]

[a] Department of Mechanical and Biofunctional Systems, Institute of Industrial Science, The University of Tokyo, 4-6-1 Komaba, Meguro-ku, Tokyo 153-8505, Japan;, Email: okabey@iis.u-tokyo.ac.jp

[b] Department of Advanced Energy, Graduate School of Frontier Sciences, The University of Tokyo, 5-1-5 Kashiwanoha, Kashiwa-shi, Chiba 277-8561, Japan

[c] Department of Advanced Energy, Graduate School of Frontier Sciences, The University of Tokyo, 5-1-5 Kashiwanoha, Kashiwa-shi, Chiba 277-8561, Japan

[d] Department of Advanced Energy, Graduate School of Frontier Sciences, The University of Tokyo, 5-1-5 Kashiwanoha, Kashiwa-shi, Chiba 277-8561, Japan

[e] Department of Advanced Energy, Graduate School of Frontier Sciences, The University of Tokyo, 5-1-5 Kashiwanoha, Kashiwa-shi, Chiba 277-8561, Japan

Version of record first published: 02 Apr 2012.

To cite this article: Yoji Okabe , Shu Minakuchi , Nobuo Shiraishi , Ken Murakami & Nobuo Takeda (2008): Smart Honeycomb Sandwich Panels With Damage Detection and Shape Recovery Functions, Advanced Composite Materials, 17:1, 41-56

To link to this article: http://dx.doi.org/10.1163/156855108X295645

VSP

Advanced Composite Materials 17 (2008) 41–56

ADVANCED COMPOSITE MATERIALS
www.brill.nl/acm

Smart Honeycomb Sandwich Panels With Damage Detection and Shape Recovery Functions

Yoji Okabe [a,*], **Shu Minakuchi** [b], **Nobuo Shiraishi** [b], **Ken Murakami** [b] **and Nobuo Takeda** [b]

[a] Department of Mechanical and Biofunctional Systems, Institute of Industrial Science, The University of Tokyo, 4-6-1 Komaba, Meguro-ku, Tokyo 153-8505, Japan

[b] Department of Advanced Energy, Graduate School of Frontier Sciences, The University of Tokyo, 5-1-5 Kashiwanoha, Kashiwa-shi, Chiba 277-8561, Japan

Received 2 November 2006; accepted 22 May 2007

Abstract

In this research, optical fiber sensors and shape memory alloys (SMA) were incorporated into sandwich panels for development of a smart honeycomb sandwich structure with damage detection and shape recovery functions. First, small-diameter fiber Bragg grating (FBG) sensors were embedded in the adhesive layer between a CFRP face-sheet and an aluminum honeycomb core. From the change in the reflection spectrum of the FBG sensors, the debonding between the face-sheet and the core and the deformation of the face-sheet due to impact loading could be well detected. Then, the authors developed the SMA honeycomb core and bonded CFRP face-sheets to the core. When an impact load was applied to the panel, the cell walls of the core were buckled and the face-sheet was bent. However, after the panel was heated over the reverse transformation finish temperature of the SMA, the core buckling disappeared and the deflection of the face-sheet was relieved. Hence the bending stiffness of the panel could be recovered.

Keywords

Honeycomb sandwich panel, optical fiber sensor, shape memory alloy, damage detection, shape recovery

1. Introduction

Honeycomb sandwich panels consist of a thick lightweight honeycomb core and two thin stiff face-sheets bonded by thin adhesive films as shown in Fig. 1. Since these panels have high specific bending stiffness, they have been applied to various lightweight structures, such as airplanes and space structures [1].

* To whom correspondence should be addressed. E-mail: okabey@iis.u-tokyo.ac.jp
Edited by the JSCM

DOI:10.1163/156855108X295645

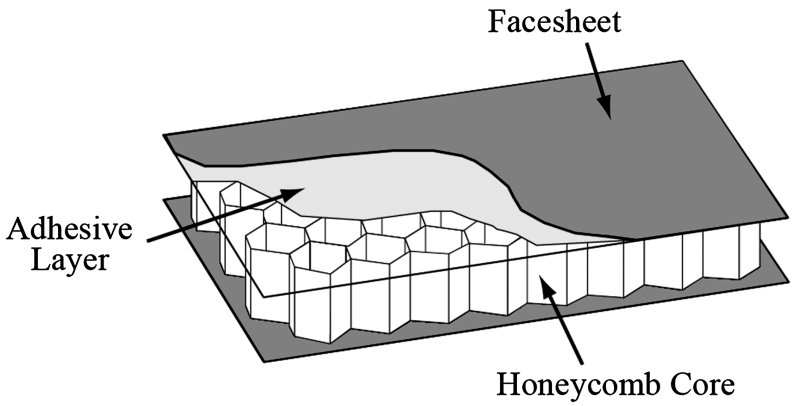

Figure 1. Honeycomb sandwich panel.

However, sandwich structures might suffer particular damage due to their vulnerability to out-of-plane loadings. Tool drops during assembling and maintenance or low-velocity collisions of small foreign objects during operation cause impact damage [2–4]. On the other hand, fatigue loads or excessive thermal stresses introduce debonding between the core and the face-sheet [5, 6]. Typical damage such as this degrades the bending stiffness and the in-plane compressive strength. For detection of such damage in airplanes, visual inspections and non-destructive tests, such as ultrasonic inspection, are applied. When they are detected, the damaged regions are hollowed out and intact cores are refilled. These inspections and the repairs need a great deal of time and effort so they need to be minimized.

Hence, in this research, the authors attempted to construct a novel smart honeycomb sandwich panel that can detect typical damage in real time and repair the deformations due to the damage easily. We embedded small-diameter optical fiber sensors in the adhesive layer between the core and the CFRP face-sheet to detect the debonding and the impact damage. Then the cell walls of the honeycomb core were made of shape memory alloy (SMA) foils to repair the out-of-plane deformation of the face-sheet caused by impact loading and recover the bending stiffness.

2. Development of Damage Detection Techniques

2.1. Observation of Damage in Sandwich Structures

The sandwich panels used in this research consisted of CFRP quasi-isotropic face-sheets (T700S/2500, Toray Industries, Inc., $[0/90/45/-45]_s$) and aluminum honeycomb core (AL 1/4-5052-.003, Showa Aircraft Industry Co., Ltd, Thickness: 10 mm), and these face-sheets and core were bonded with epoxy adhesive films (REDUX312UL, Hexcel).

First, low-velocity impact loading was applied to the specimen with the dimensions of $100 \times 100 \times 12$ mm^3 using a drop-weight tester (Mini-Tower, Instron). The cross-section of the specimen subjected to the impact is shown in Fig. 2. The core

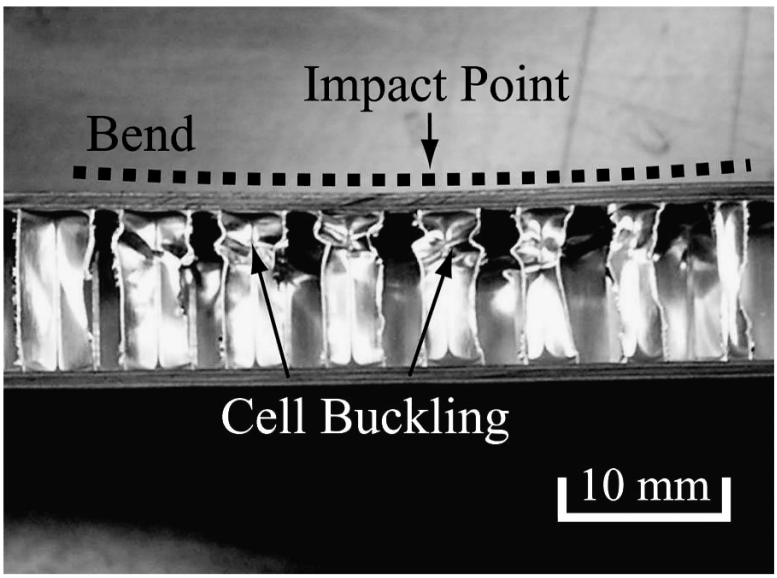

Figure 2. Impact damage.

cells beneath the impact region were buckled and pulled down the upper face-sheet. Hence the face-sheet had a gentle bend. On the other hand, when an impact loading was applied to the cylindrical indenter penetrating through a small hole made in the upper face-sheet [7], a debonding between the lower CFRP face-sheet and the core occurred (Fig. 3). In this picture, the removed core wall was also drawn additionally to illustrate the relation between the core wall and the fillet. It is observed that fillets [6] are made of the adhesive at the root of the core walls and the greater part of the fillet was debonded from the face-sheet.

2.2. Debonding Detection Using FBG Sensors

2.2.1. Embedment of Optical Fiber Sensors

At first, a fiber Bragg grating (FBG) sensor, which is a kind of optical fiber sensor, was embedded in the adhesive layer between the core and the face-sheet to detect the debonding. FBG sensors were fabricated in single-mode optical fibers to have a periodic variation in the refractive index along a certain length of the core in which light propagates. When a broadband light is injected into the core, the FBG reflects a narrow spectral component at the Bragg wavelength depending on the grating period and the effective refractive index, and the other components transmit through the FBG [8]. Hence, when non-uniform strain is applied to the grating, the distributions of the grating period and the refractive index also become non-uniform, and the reflection spectrum of the FBG is deformed because of the reflection of various wavelength components due to the non-uniformity. Using this phenomenon, the authors succeeded in detecting microscopic damage in CFRP laminates [9–12]. In this research, non-uniform thermal residual strain is already applied to the FBG sensor

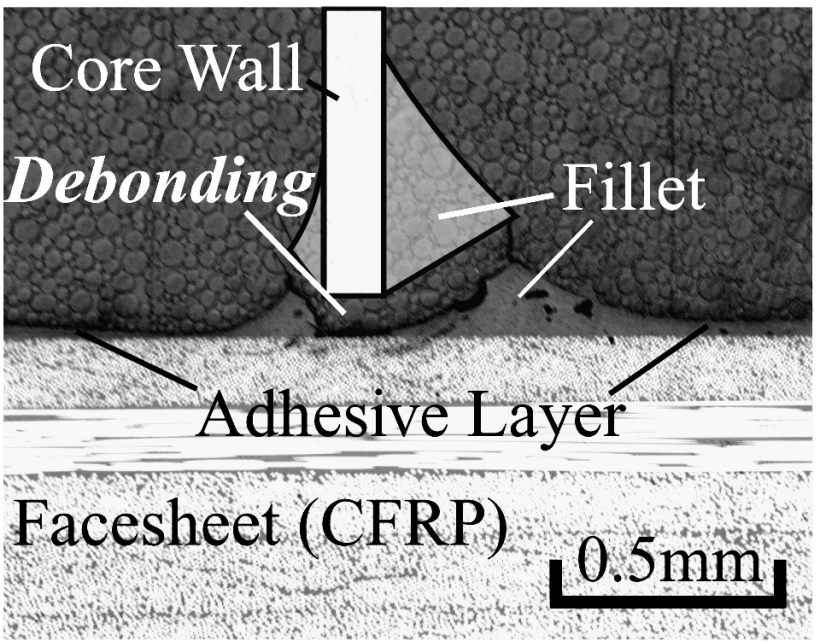

Figure 3. Debonding between the face-sheet and the core.

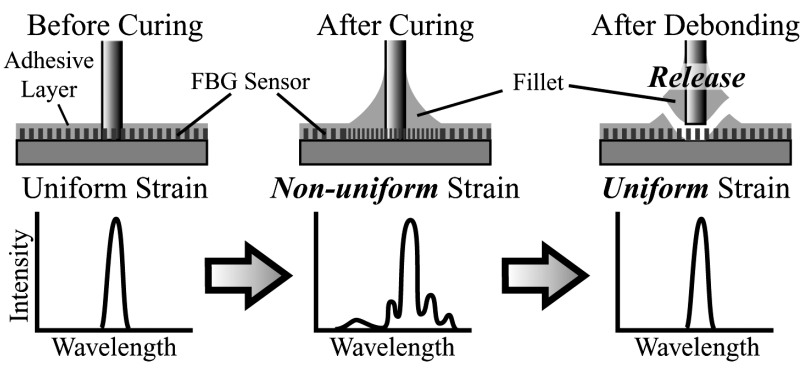

Figure 4. Principle of debonding detection using an FBG sensor.

after curing of the adhesive because of the formation of fillets as shown in Fig. 4, and the non-uniform strain is released after debonding. Hence, the recovery of the original shape of the reflection spectrum is used for the debonding detection.

A small-diameter FBG sensor (core diameter: 6.5 μm, cladding diameter: 40 μm, polyimide coating diameter: 52 μm, grating length: 10 mm) [13] was embedded in the adhesive layer between the lower face-sheet and the core. The center of the FBG was positioned just below a cell wall (Fig. 5). However, when the optical fibers are embedded in the adhesive layer, there is no space for the optical fiber to run through because the cell walls contact with the face-sheet. Hence, micro-slits were formed

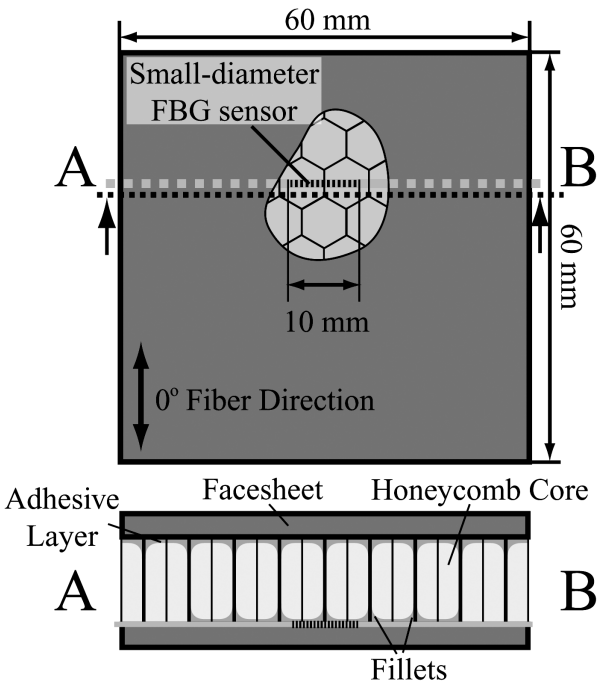

Figure 5. Embedment position of an FBG sensor in a panel.

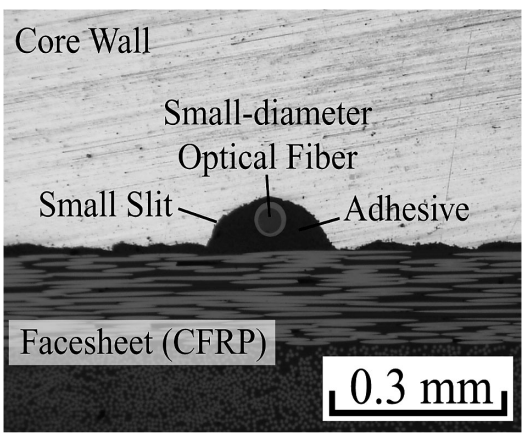

Figure 6. Small slit formed on the edge of the cell walls for embedding of an optical fiber.

in the core walls by a wire discharge cutter, and the optical fiber was embedded in the slits as shown in Fig. 6. Then adhesive films and preformed CFRP face-sheets were put on the upper and lower surfaces of the core, and the adhesive was cured under pressure at 125°C for 3 h.

2.2.2. Observation of the Reflection Spectrum During the Manufacturing Process

Since the fillets are formed while the adhesive is cured, the reflection spectrum from the FBG was observed during the curing process using an ASE light source (AQ4319(155), Ando Electric Co. Ltd.) and an optical spectrum analyzer (AQ6317, Ando Electric Co. Ltd.). The observed spectra are depicted in Fig. 7. The intensity of each reflection spectrum was normalized by the intensity of the highest component. At room temperature of 25°C before curing, the spectrum had only one sharp narrow peak. Also at curing temperature of 125°C, the spectrum retained its original shape and the center wavelength shifted to longer wavelength corresponding to the temperature increase. However, at room temperature after the curing, the form of the spectrum was obviously distorted. This is due to the thermal residual strain caused by the fillet formed at 125°C, because the center of the 10 mm FBG was just below the core wall. Hence it is expected that the spectrum will recover its original shape when the non-uniform residual strain is released by debonding of the core with the fillets from the face-sheet.

2.2.3. Flatwise Tensile Test to Introduce Debonding

Then, a flatwise tensile test was conducted to debond the lower face-sheet from the core and the change in the reflection spectrum of the embedded FBG during the test was observed. The flatwise tensile test is the most general for evaluating the adhesive strength of a sandwich structure by applying uniform out-of-plane tensile stress on both face-sheets. Each face-sheet of the specimen was bonded to an aluminum block and loaded by a material testing system (AG-I, Shimadzu Corp.). The reflection spectra measured during this test are shown in Fig. 8. After the debonding, the components separate from the maximum peak disappeared, and the spectrum almost recovered its original shape. Hence, the occurrence of the debonding is expected to be detected from the change in the spectrum shape.

2.2.4. Theoretical Simulation

In order to confirm this phenomenon, a theoretical simulation was conducted. First, the triaxial strain distribution applied on the optical fiber before and after debonding was calculated using 3D finite element analysis (FEA) with ABAQUS code. All of the CFRP face-sheet, the aluminum honeycomb core, the adhesive layer, the fillets,

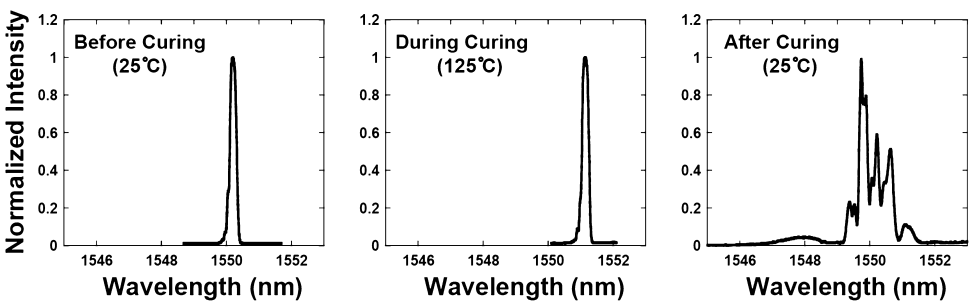

Figure 7. Reflection spectra measured during the curing process of the adhesive films.

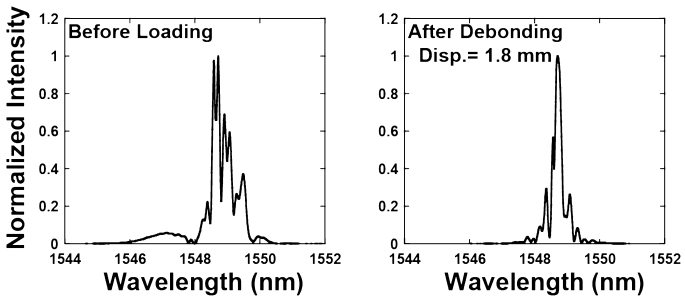

Figure 8. Change in the spectrum due to the debonding through a flatwise tensile test.

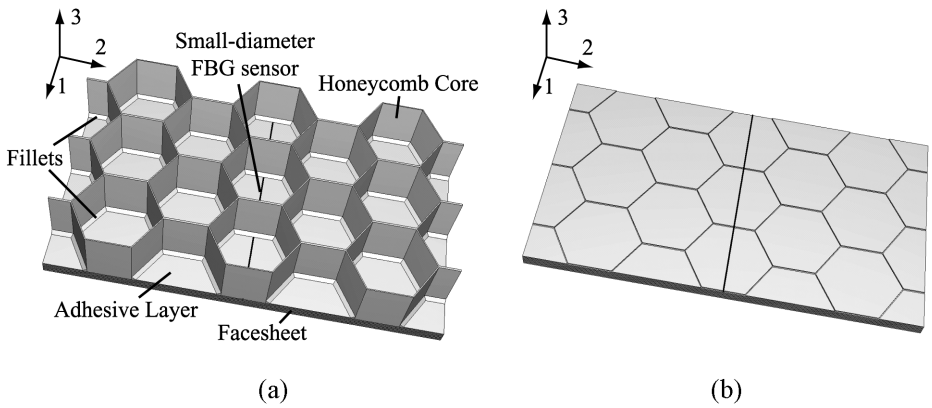

Figure 9. FEM models to calculate the change in the strain distribution due to the debonding: (a) intact plate and (b) debonded face-sheet.

and the small-diameter optical fiber were modeled in detail using solid elements as illustrated in Fig. 9. The height and width of the fillets in the x_3 and x_1 directions, respectively, were set to be 300 μm, which was determined from cross-sectional observation of the specimen used for the experiment [14]. The material properties of the components are listed in Table 1. Then, the distributions of the effective refractive index and the grating period of the FBG were obtained from the triaxial strain distribution, and the reflection spectrum of the FBG was simulated using couple mode theory and the transfer matrix method from the distributions [15].

The triaxial strain of the FBG sensor calculated by the FEA is plotted in Fig. 10. These results show that large non-uniformity of the strain appears around the fillet and is relieved by the debonding. Then, the calculated spectra are shown in Fig. 11. After the debonding, the disturbance of the spectrum caused by the fillet disappeared and the spectrum almost recovered its original shape. Since this change agreed well with that of the experimental results, the deformation in the spectrum was confirmed to be due to the thermal residual strain of fillets. Thus, the debonding detection is possible by monitoring of the spectrum shape.

Table 1.
Material properties of T700S/2500 unidirectional laminates, aluminum 5052, REDUX312UL and small-diameter optical fiber

		T700S/2500	Aluminum 5052	REDUX 312UL	Small-diameter optical fiber	Polyimide coating
Elastic moduli (GPa)	E_1	130.1	69.3	3.5	73.1	1.5
	E_2	8.03				
	G_{12}	4.8				
Poisson's ratios	ν_{12}	0.31	0.33	0.3	0.16	0.25
	ν_{23}	0.49				
Thermal expansion coefficients ($\times 10^{-6}$/°C)	α_{11}	0.3	23.8	46	0.5	15
	α_{22}	36.5				

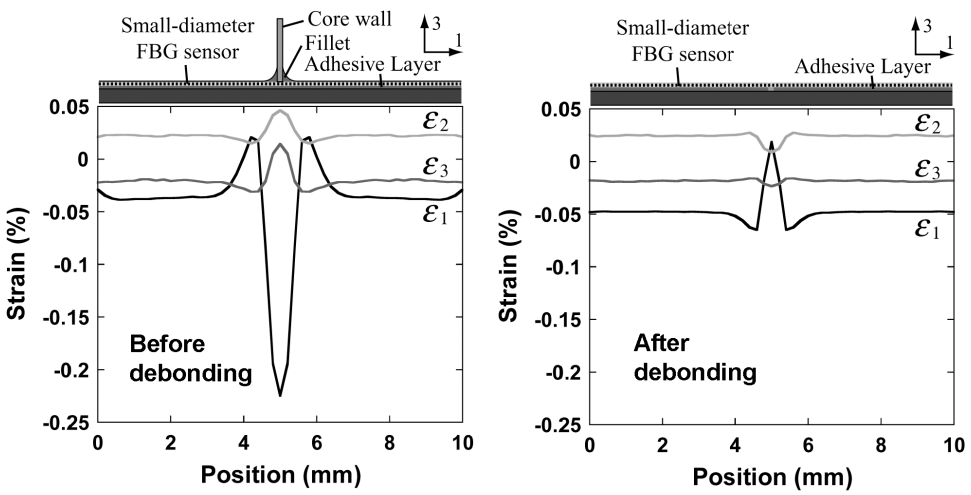

Figure 10. Strain distributions along the central axis of the optical fiber before and after the debonding.

2.3. Detection of Impact Damage

Next, the detection of the impact damage caused by a low-velocity impact loading was attempted. In this technique, strain distribution over long distance of about 50 mm should be considered because the bend of the face-sheet is very gentle. If uniform FBG is formed with long grating length, the spectrum width becomes very narrow, so that the observation of the change in the spectrum form becomes difficult. Hence, chirped FBG sensors [16] of 50 mm in grating length and 5 nm in spectrum width were applied. The difference between the uniform FBG and the chirped FBG are illustrated in Fig. 12. Since the grating period of the chirped FBG increases monotonically within the gauge length, the reflection spectrum from the chirped FBG is very broad and the wavelength in the spectrum is expressed as a

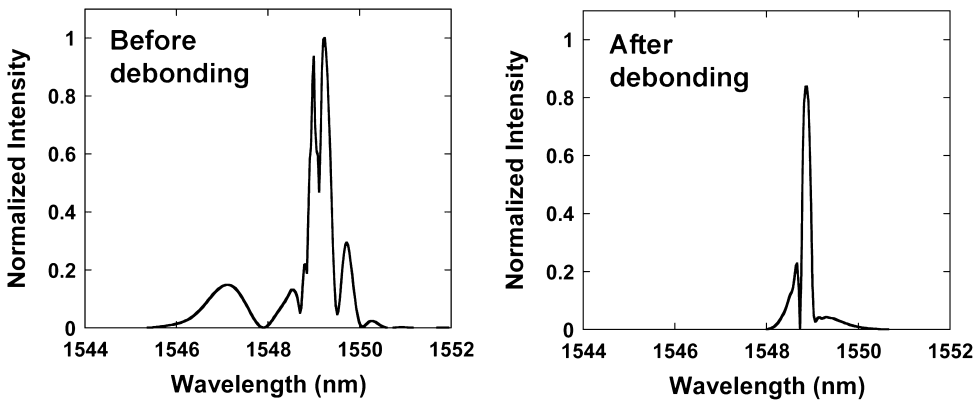

Figure 11. Reflection spectra calculated from the strain distributions in Fig. 10.

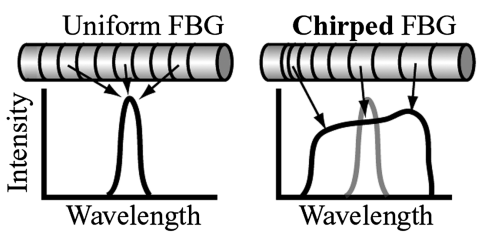

Figure 12. Comparison between a uniform FBG and a chirped FBG.

function of the position along the grating. Hence the location of strain fluctuation can be estimated directly from the reflection spectrum [16]. In this research, the chirped FBG sensor is expected to respond to the deformation of the face-sheet due to the impact load. Also, this sensor is anticipated to be effective for the debonding detection mentioned in the previous section.

We embedded the chirped FBG sensor in the upper adhesive layer, positioning the longest grating period end of the FBG in the center of the specimen of 100 mm × 100 mm. The reflection spectrum of the embedded chirped FBG is shown in Fig. 13. In this spectrum, eight dips appeared periodically. This is because eight fillets exist at about 6 mm intervals periodically in the grating length of 50 mm and the residual strain of the fillets causes these disturbances.

For this sandwich panel, impact load was applied to the center of the upper face-sheet using the drop-weight tester as shown in Fig. 14. In this figure, the longest period of the chirped FBG is represented by white and the shortest period is shown in black, and the distribution of the grating period is expressed as the gradation. When the upper face-sheet is deformed by an impact load, the lower surface at the convex region of the face-sheet is compressed and the shorter grating period becomes much shorter. On the other hand, that at the concave region is stretched and the longer grating period becomes much longer [17]. Hence, it is expected that the reflection spectrum changes as drawn in Fig. 14.

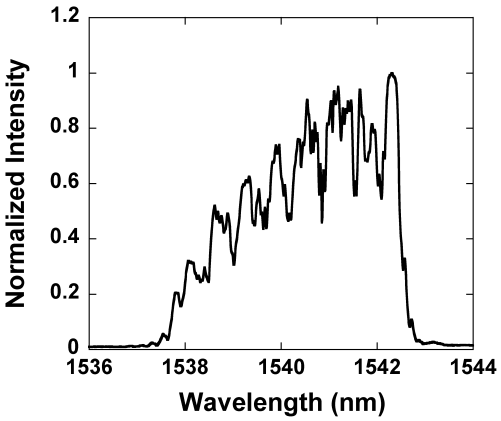

Figure 13. Reflection spectrum from the chirped FBG sensor embedded in the sandwich panel.

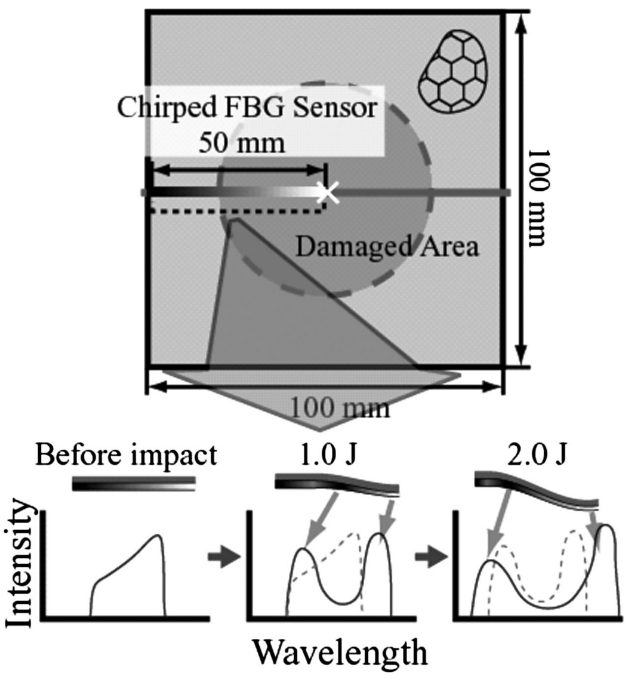

Figure 14. Configuration of the impact test and the expected change in the reflection spectrum.

Actually, an impact energy of 1.0 J or 2.0 J was applied to the center of the specimen. After the impact loadings, the out-of-plane displacements of the face-sheets were measured with a CCD laser displacement sensor (LK-030, Keyence), and the reflection spectra from the embedded chirped FBG sensors were observed. The deformation of the face-sheet is shown in Fig. 15. With an increase in the impact energy, the dent in the face-sheet became deeper and wider. The reflection spectra in both cases are shown in Fig. 16. Compared with the spectrum in Fig. 13,

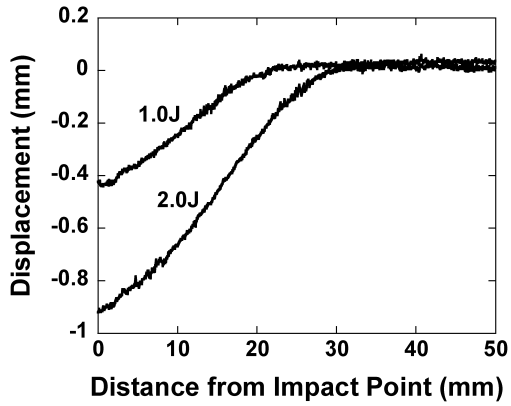

Figure 15. Deformations of the face-sheet after impact loadings.

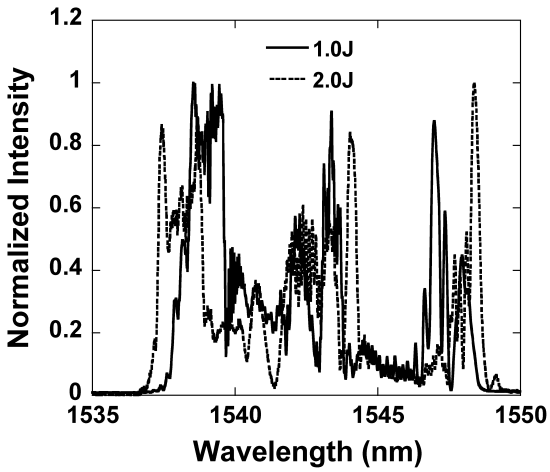

Figure 16. Measured reflection spectra of the chirped FBG sensors after impact loadings.

after impact loading, the long wavelength components shifted to longer wavelength and the short ones to shorter wavelength, so that the spectrum became broader. These results indicate that the impact damage can be detected quantitatively from the change in the shape and width of the spectrum.

3. Shape Recovery Using SMA Honeycomb

As shown in Fig. 15, when an impact loading is applied to the sandwich panel, the upper face-sheet is bent in the out-of-plane direction. This deformation is caused by the pull down due to the buckled cell walls beneath the impact region as shown in Fig. 2. Thus the distance between the upper and the lower face-sheets becomes shorter and the moment of inertia of the cross-section decreases. In consequence, the bending stiffness decreases in proportion to the square of the distance between

the face-sheets. However, since the bending is elastic deformation while the impact energy is small, the face-sheet will return to a flat plate if the cell buckling is repaired.

The actuator to repair the cell buckling needs the following properties: (a) light weight, (b) large actuating force and displacement, and (c) without lead wires. Thus the authors selected a shape memory alloy (SMA) as the actuator material. However, if the actuator is embedded in the core cell and generates the actuating force in the thickness direction, there is a risk of debonding initiation. Hence we attempted to make the cell walls of SMA foils (Ti-50.2% Ni, Furukawa Electric Co. Ltd., Thickness: 45 μm) [18]. At first, in order to make the SMA foil memorize the honeycomb shape, the SMA foil was put between two pieces of metal mould, whose shape is an array of half hexagons, and heated at 400°C for 1 h. After the shape memorization, the SMA foils were glued with adhesive (modified silicone) to form the honeycomb core (Fig. 17(a)).

An impact loading was applied to the center of the SMA honeycomb core, and the cell walls around the center were buckled as shown in Fig. 17(b). After that, the specimen was heated in a thermostatic chamber up to 80°C that was over the reverse transformation finish temperature. The buckling of the core walls disappeared and

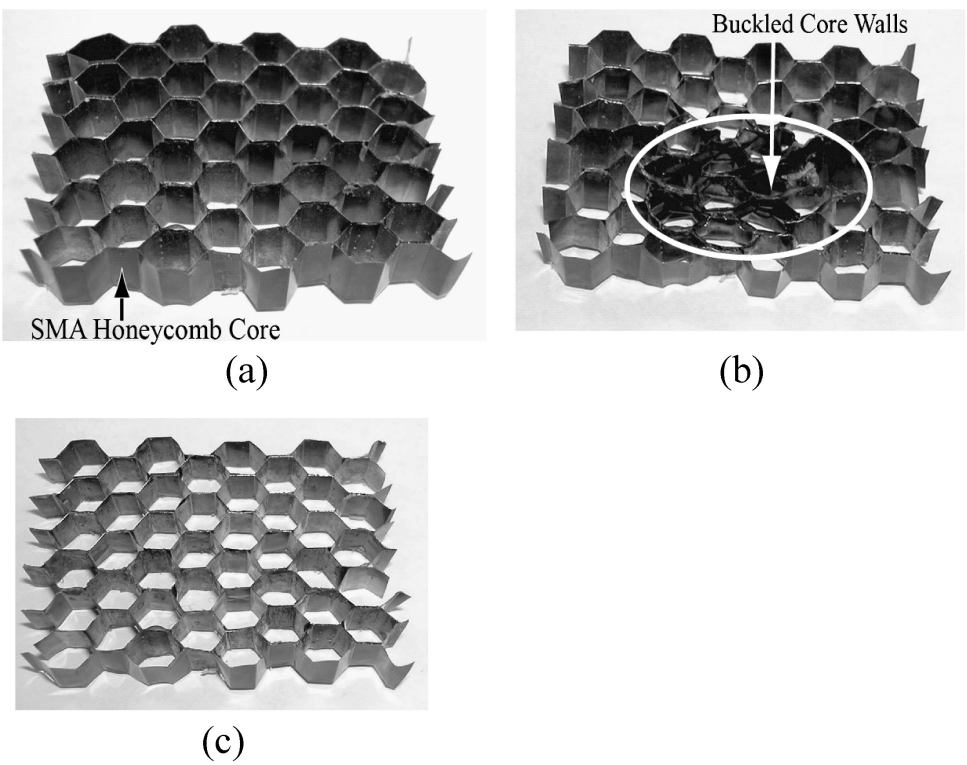

Figure 17. Honeycomb core made of SMA foils: (a) before impact loading, (b) after impact loading and (c) after heating.

the shape of the honeycomb was completely recovered to that before impact loading (Fig. 17(c)).

Next, CFRP cross-ply laminates ([0/90/90/0], Thickness: 0.5 mm) were bonded as face-sheets to the SMA honeycomb core of 10 mm in thickness using the epoxy adhesive films. The dimensions of the SMA honeycomb sandwich panel were 150 mm × 30 mm × 11 mm. For this panel, an impact energy of 3.0 J was applied using the drop-weight tester to cause an impact damage. Then the panel was heated up to 80°C for the shape recovery. At all steps, before and after impact loading and after heating, a four-point bending test with the configuration illustrated in Fig. 18 was carried out to the panel to measure the load–displacement curve whose slope relates to the average bending stiffness.

The photographs of the sandwich panel taken at all steps are shown in Fig. 19. The out-of-plane displacements of the upper face-sheet measured with the laser

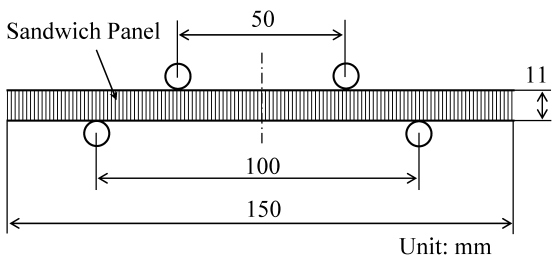

Figure 18. Schematic of four-point bending test.

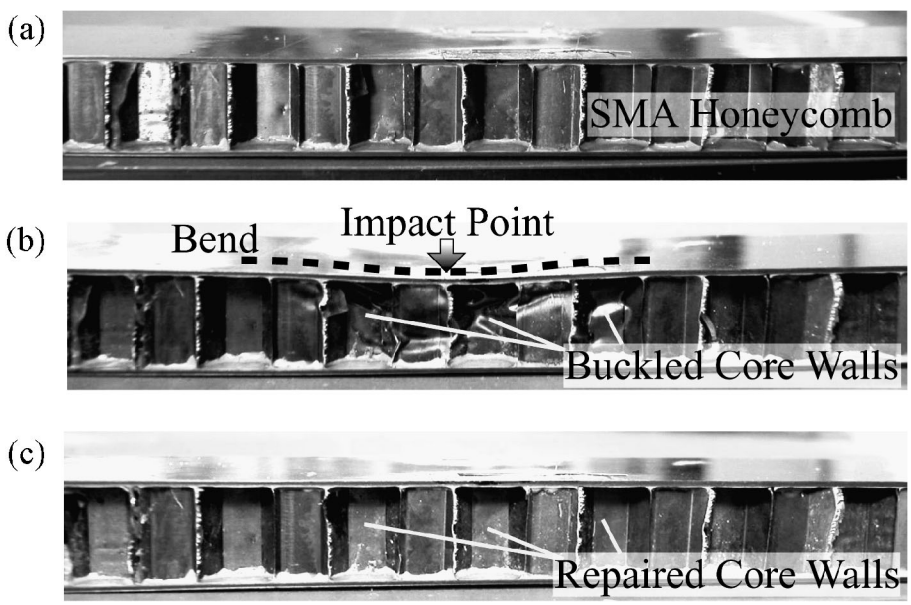

Figure 19. SMA honeycomb sandwich panel: (a) before impact loading, (b) after impact loading and (c) after heating.

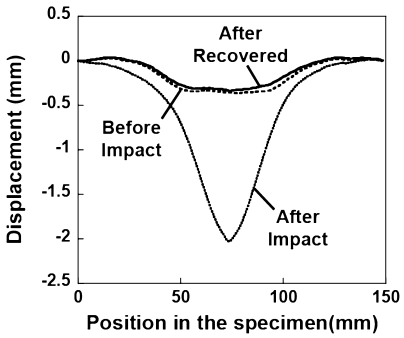

Figure 20. Out-of-plane displacements of the upper surface.

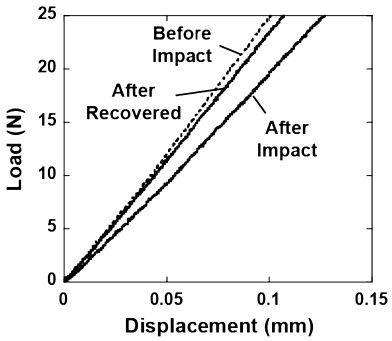

Figure 21. Load–displacement curves obtained from the four-point bending tests.

displacement sensor are plotted in Fig. 20. Furthermore, Fig. 21 shows the load–displacement curves measured by the four-point bending tests. Although the slight deformation of the surface appeared already before impact loading due to the low precision of the manufacturing, this initial imperfection did not affect this experiment. From Figs 19 and 20, it was found that the cell walls were buckled locally and the upper face-sheet was bent after the impact loading. By heating, however, the core buckling disappeared and the face-sheet recovered its original shape. With this deformation, the bending stiffness also changed. Figure 21 indicates that the bending stiffness decreased by the impact damage and returned almost to the initial value after heating. Hence, the shape restoration of the upper face-sheet leads to recovery of the bending stiffness and has a potential to suppress the further damage progress.

4. Conclusions

At first, the authors developed detection techniques for typical damage in sandwich panels consisting of CFRP face-sheets and aluminum honeycomb core with small-diameter FBG sensors. When debonding appeared between the face-sheet and the core, the reflection spectrum from the embedded FBG sensor returned to its original

shape from the spectrum disturbed by the non-uniform thermal residual strain of fillets. Then, when the impact damage occurred, the reflection spectrum from the embedded chirped FBG became broader depending on the impact energy. Thus the debonding and the impact damage could be detected by monitoring of the spectrum shape. However, these techniques have a drawback that only the damage in the vicinity of the FBG sensor can be detected. Hence the authors are also attempting to use the change in transmitted optical powers caused by local bending or breakage of small-diameter optical fibers for debonding detection [19]. If these techniques are combined, debondings will be detected in a much larger area more robustly. In addition, we also introduced a MEMS-optical spectrum analyzer [20] that can measure the reflection spectrum at very high speed. If the change in the reflection spectrum can be observed during impact loadings, the impact location and damage magnitude will be identified [21].

On the other hand, the cell walls of the honeycomb core were made of SMA foils for the recovery of the bending stiffness degraded by impact damage, and CFRP face-sheets were bonded to the SMA honeycomb core. When an impact load was applied to the SMA honeycomb sandwich panel, the cell walls of the core were buckled and the face-sheet was bent. However, after the panel was heated over the reverse transformation finish temperature of the SMA, the core buckling disappeared and the deflection of the face-sheet was relieved. With the shape restoration, the bending stiffness of the panel could be recovered.

Through the integration of these techniques, a smart honeycomb sandwich panel can be constructed, which can detect damages and recover the mechanical properties for suppression of further damage progress.

Acknowledgement

This study was supported by the 2003 Industrial Technology Research Grant Program from the New Energy and Industrial Technology Development Organization (NEDO) of Japan.

References

1. D. Zenkert (Ed.), *The Handbook of Sandwich Construction*. EMAS Publishing, Warrington, UK (1997).
2. S. Abrate, Localized impact on sandwich structures with laminated facings, *Appl. Mech. Rev*. **50**, 69–82 (1997).
3. T. Anderson and E. Madenci, Experimental investigation of low-velocity impact characteristics of sandwich composites, *Compos. Struct*. **50**, 239–247 (2000).
4. E. J. Herup and A. N. Palazotto, Low-velocity impact damage initiation in graphite/epoxy/Nomex honeycomb-sandwich plates, *Compos. Sci. Technol*. **57**, 1581–1598 (1997).
5. A. Ural, A. T. Zehnder and A. R. Ingraffea, Fracture mechanics approach to face-sheet delamination in honeycomb: measurement of energy release rate of the adhesive bond, *Engng Fract. Mech*. **70**, 93–103 (2003).

6. R. Okada and M. T. Kortschot, The role of the resin fillet in the delamination of honeycomb sandwich structures, *Compos. Sci. Technol*. **62**, 1811–1819 (2002).
7. E. Blaise and F.-K. Chang, Built-in diagnostics for debonding in sandwich structures under extreme temperatures, in: *Structural Health Monitoring — The Demands and Challenges*, F.-K. Chang (Ed.), pp. 154–163. CRC Press, Boca Raton, USA (2001).
8. A. D. Kersey, M. A. Davis, H. J. Patrick, M. LeBlanc, K. P. Koo, C. G. Askins, M. A. Putnam and E. J. Friebele, Fiber grating sensors, *J. Lightwave Technol*. **15**, 1442–1463 (1997).
9. Y. Okabe, S. Yashiro, T. Kosaka and N. Takeda, Detection of transverse cracks in CFRP composites using embedded fiber Bragg grating sensors, *Smart Mater. Struct*. **9**, 832–838 (2000).
10. S. Takeda, Y. Okabe and N. Takeda, Delamination detection in CFRP laminates with embedded small-diameter fiber Bragg grating sensors, *Composites, Part A* **33**, 971–980 (2002).
11. T. Mizutani, Y. Okabe and N. Takeda, Quantitative evaluation of transverse cracks in carbon fiber reinforced plastic quasi-isotropic laminates with embedded small-diameter fiber Bragg grating sensors, *Smart Mater. Struct*. **12**, 898–903 (2003).
12. S. Takeda, Y. Okabe, T. Yamamoto and N. Takeda, Detection of edge delamination in CFRP laminates under cyclic loading using small-diameter FBG sensors, *Compos. Sci. Technol*. **63**, 1885–1894 (2003).
13. K. Satori, K. Fukuchi, Y. Kurosawa, A. Hongo and N. Takeda, Polyimide-coated small-diameter optical fiber sensors for embedding in composite laminate structures, in: *Smart Structures and Materials 2001, Proc. SPIE*, Vol. 4328, E. Udd and D. Inaudi (Eds), pp. 285–294. SPIE, Bellingham, UK (2001).
14. S. Minakuchi, Y. Okabe and N. Takeda, Real-time detection of debonding between honeycomb core and face-sheet using a small-diameter FBG sensor embedded in adhesive layer, *J. Sandwich Struct. Mater*. **9**, 9–33 (2007).
15. A. Othonos and K. Kalli, *Fiber Bragg Gratings: Fundamentals and Applications in Telecommunications and Sensing*, Chapter 5. Artech House, Boston, USA (1999).
16. Y. Okabe, R. Tsuji and N. Takeda, Application of chirped fiber Bragg grating sensors for identification of crack locations in composites, *Composites, Part A* **35**, 59–65 (2004).
17. L. J. Lee, K. Y. Huang and Y. J. Fann, Dynamic response of composite sandwich plate impacted by a rigid ball, *J. Compos. Mater*. **27**, 1238–1256 (1993).
18. I. Taketa, M. Amano, M. Kobayashi, T. Ogisu, Y. Okabe and N. Takeda, Modeling of thermomechanical behavior of Ti–Ni shape memory alloy foils embedded in carbon fiber reinforced plastic laminates, *Adv. Composite Mater*. **14**, 25–42 (2005).
19. S. Minakuchi, Y. Okabe and N. Takeda, Real-time damage detection of honeycomb sandwich structures using small-diameter fiber Bragg grating sensors, in: *Proc. 7th International Conference on Sandwich Structures (ICCS-7)*, pp. 383–392. Springer, Dordrecht, The Netherlands (2005).
20. Y. Takahashi, High speed MEMS-OSA and its application to fiber sensors, in: *Second European Workshop on Optical Fiber Sensors, Proc. SPIE*, Vol. 5502, J. M. Lopez-Higuera and B. Culshaw (Eds), pp. 33–38. SPIE, Bellingham, UK (2004).
21. Y. Okabe, S. Minakuchi and N. Takeda, Identification of impact damage in sandwich structures by application of high speed MEMS-OSA to FBG sensors, in: *Smart Structures and Materials 2005, Proc. SPIE*, Vol. 5758, E. Udd and D. Inaudi (Eds), pp. 105–113. SPIE, Bellingham, UK (2005).